Wide-Angle Reflective Terahertz Beam Steering Metasurface Based on Cross-Polarization Conversion

Mengyao Li, *Member, IEEE*, Zhonghua Gu, Cheemalamarri Hemanth Kumar, Nanhan Liu, Frédéric Dutin, Pascal Szriftgiser, Guillaume Ducournau, *Member, IEEE*, and Prakash Pitchappa, *Member, IEEE*

***Abstract*—The terahertz (THz) frequency range is considered an important spectrum for future 6G communication. However, the high propagation losses and poor penetration inherent to terahertz waves restricted its development. Wavefront manipulation techniques for beam steering to redirect the propagation directions are essential for mitigating these limitations. In this paper, cross-polarization conversion-based phase engineering for THz reflective beam steering is presented. This approach has the advantages of enabling quasi-linear phase response with sufficient phase shifting range and maintaining high reflection magnitudes over a wide frequency band. Furthermore, a four ports equivalent circuit is developed to explain the design principle and verify the effectiveness of the polarizers. As a result, the metasurfaces composed of the proposed unit cells achieve stable wide-angle beam steering with high reflection intensity and have continuous frequency-scanning capability. In addition, the metasurfaces are verified to support high-quality 16-QAM modulation with acceptable power penalty in a non-line-of-sight THz link.**

***Index Terms*—Beam steering metasurface, cross-polarization converter, six-generation (6G), terahertz communications.**

Manuscript received August 2025; revised XXX; accepted XXX. This work is supported by A*STAR MTC Programmatic grant no M22L1b0110. This work is also supported by the France 2030 programs, CPER Wavetech. The PEPR is operated by the Agence Nationale de la Recherche (ANR), under the grants ANR-22-PEEL-0006 (FUNTERA, PEPR 'Electronics') and ANR-22-PEFT-0006 (NF-SYSTERA, PEPR 5G and beyond - Future Networks). The Contrat de Plan Etat-Region (CPER) WaveTech is supported by the Ministry of Higher Education and Research, the Hauts-de-France Regional council, the Lille European Metropolis (MEL), the Institute of Physics of the French National Centre for Scientific Research (CNRS) and the European Regional Development Fund (ERDF). This work is also supported by French RENATECH network, the Equipex+ Nanofutur operated by the ANR, under the grant IA-21-ESRE-0012. The authors acknowledge support from CDP C2EMPI, the French State under the France-2030 program, the University of Lille, the Initiative of Excellence of the University of Lille, the European Metropolis of Lille for their funding and support of the R-CDP-24-004-C2EMPI project. *(Corresponding author: Prakash Pitchappa.)*

Mengyao Li, Zhonghua Gu, Cheemalamarri Hemanth Kumar, Nanhan Liu, and Prakash Pitchappa are with the Institute of Microelectronics, Agency for Science, Technology and Research, Singapore, 138634 (email: Prakash_Pitchappa@a-star.edu.sg).

Frédéric Dutin and Guillaume Ducournau are with the University of Lille, CNRS, Centrale Lille, Univ. Polytechnique Hauts-de-France, UMR 8520-IEMN, Institut d'Electronique de Microélectronique et de Nanotechnologie, 59000 Lille, France. (email : guillaume.ducournau@univ-lille.fr)

P. Szriftgiser is with University of Lille, CNRS, Laboratoire de Physique des Lasers, Atomes et Molécules, PhLAM, UMR 8523, F-59000 Lille, France.

I. Introduction

THE terahertz (THz) frequency band has become an important candidate for future sixth generation (6G) wireless communication systems due to its potential for extremely high data rates [1]-[3]. However, THz waves inherently suffer from high propagation loss and poor diffraction capability, which significantly limit their propagation range [4]-[6]. To mitigate such high path losses, THz systems typically employ highly directional beams to improve the signal-to-noise ratio (SNR). While such a strategy improves link performance, it significantly reduces spatial coverage for multi-user scenarios. Therefore, beam steering technologies, which can redirect the THz beams toward different locations, have become essential for THz communication systems. Conventionally, phased array antennas are widely used for beam steering applications. However, they suffer from high hardware complexity and large power consumption at THz frequencies [7]-[9]. Optical feed–THz phased systems have also been investigated, but they typically rely on optical components, which hinder compact integration [10], [11]. Recently, metasurfaces have attracted increased attention as they can manipulate electromagnetic wavefronts with subwavelength resolution [12], [13]. Its unique advantages of passive operation, ease of integration, and compact structures make them well-suited for THz wireless system [14].

To achieve beam steering with metasurfaces, the subwavelength elements distributed on the surface should retain specific phase differences. Numerous studies focus on implementing the desired phase response and sufficient phase shifting range. One straightforward approach is to utilize various structural thicknesses to introduce optical path differences and thereby generate phase differences [15], [16]. However, this method often needs bulky and complex structures, which is especially problematic for high-frequency applications [17]-[19]. Another effective and widely used technique is resonance shifting, which achieves phase shift by adjusting the resonant frequency of the unit cell. However, they only provide precise phase control at a single operating frequency [20]-[24]. So, the steering angle changes unpredictably with frequency, thereby making frequency-scanning functionality that enables continuous beam steering across the operating frequency range extremely difficult [25],

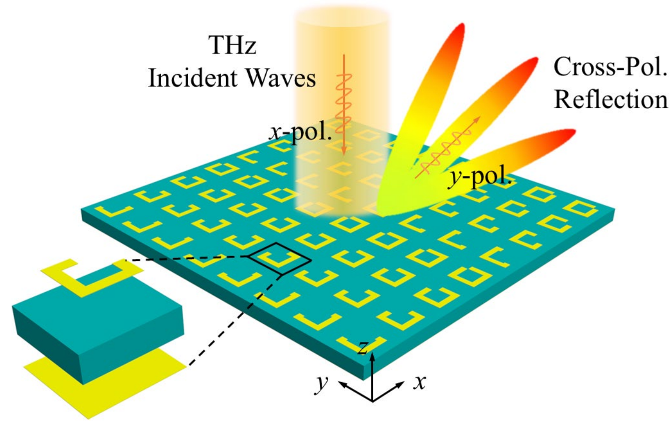

Fig. 1. Conceptual depiction of the proposed metasurface based on cross-polarization converters.

[26]. Frequency-scanning, however, plays a critical role in terahertz applications such as high-resolution imaging, non-destructive testing, and security screening [27], [28]. Furthermore, it is also difficult to achieve a full 360° phase shift range and maintain high reflection magnitude across all phase states simultaneously [29]-[31]. Hence, there is a trade-off between the phase coverage and amplitude uniformity, which affects the stability and efficiency of these metasurfaces and demands higher fabrication accuracy.

To alleviate the above limitations, the concept of polarization conversion has been introduced into metasurface design. Its unique advantage is that the required phase shifting range can be reduced by half, from 360° to 180°, because the other half can be easily compensated by controlling the rotated electrical field direction [25]. The polarization conversion strategy has been effectively adopted in the radio frequency range for various applications to assist phase control and then achieve wavefront manipulation, such as transmitarrays [32]-[34], reflectarrays [35], [36], orbital angular momentum (OAM) and beam generation [37], [38]. In the THz frequency range, some designs for polarization converters have been proposed with improved conversion efficiency, broadened bandwidth, and higher angular stability [39]-[43]. However, the application of polarization converters for beam steering still suffers from low efficiency and limited phase control [44], [45].

In this paper, a 3-bit metasurface based on the polarization conversion design concept for wide-angle beam steering operating in the THz band is presented. Eight types of unit cells with a 45° phase gradient are designed to cover the full 360° phase shifting range. With the help of polarization conversion, all unit cells exhibit high reflection magnitudes exceeding 0.8 across a relatively wide frequency band from 266 GHz to 323 GHz, rather than at a single frequency, hence overcoming the typical trade-off between phase coverage and amplitude stability. Furthermore, these unit cells exhibit similar slopes of phase with respect to frequency, which is essential for continuous and predictable frequency scanning. In addition, the proposed metasurface is verified by a non-line-of-sight THz wireless link, supporting quadrature amplitude modulation with 16 states (16-QAM) [46]. The experimental results highlight the practical potential of polarization conversion based metasurfaces in future THz wireless networks.

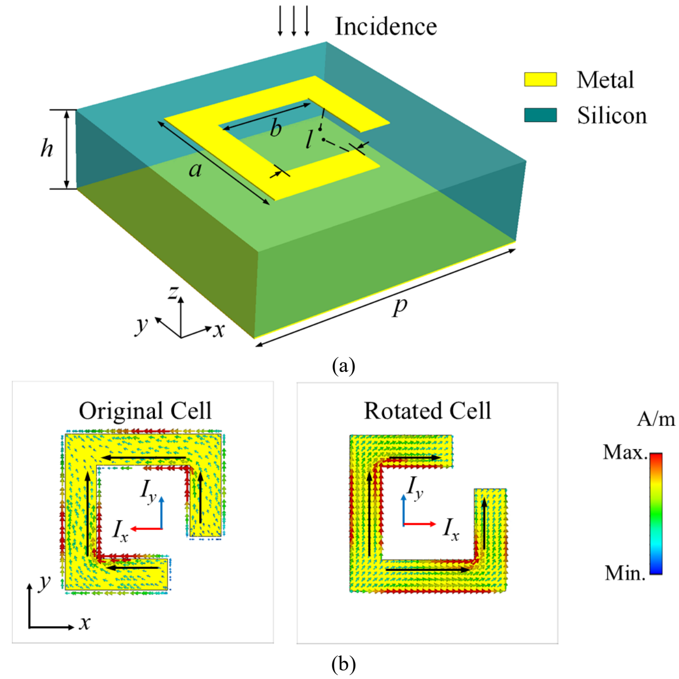

Fig. 2. Unit cell structure of the phase controllable polarization converter. (a) Perspective view of the unit cell. (b) Current distribution of the "Original Cell" and the "Rotated Cell". (Dimension: p = 210 μm, h = 60 μm, a = 125 μm, b = 75 μm, l = variation.)

II. Design and Analysis

The proposed design concept is shown in Fig. 1. The metasurface is based on cross-polarization converters, which reflects the incident *x*-polarized (*y*-polarization) THz waves in *y*-polarization (*x*-polarized). The structure includes metallic patterns on a single-crystalline silicon spacer backed with a reflecting ground. By adjusting the size of the patterns, a large phase shifting range can be achieved, while the reflection magnitudes remain high. As a result, the reflected beam can be steered in the non-specular directions, which can be controlled over a wide-angular range.

A. Unit Cell Design

For the ideal 3-bit reflective metasurface design, 8 unit cells with a uniform phase gradient of 45° and unity reflection magnitude are needed. As mentioned before, the phase shifting range that needs to be considered can be reduced by half using the design concept of cross-polarization conversion. Therefore, the unit cells that need to be designed are reduced from 8 to 4.

The proposed unit cell structure is based on a notched square ring composed of 1 μm thick Aluminum (Al) fabricated on 60 μm thick high-resistivity silicon spacer with a 1 μm thick reflecting Al ground as shown in Fig. 2(a). To obtain the desired phase response, the length of the split arms (value of l) is varied. The asymmetry in the proposed unit cell allows for conversion of incident co-polarized waves to cross-polarized reflected waves with a high cross-polarized reflection magnitude. The frequency responses are identical for the proposed unit cell under *x*- and *y*-polarized normal incidence. In this work, the *x*-polarized plane wave is chosen as the incident source in the measurements.

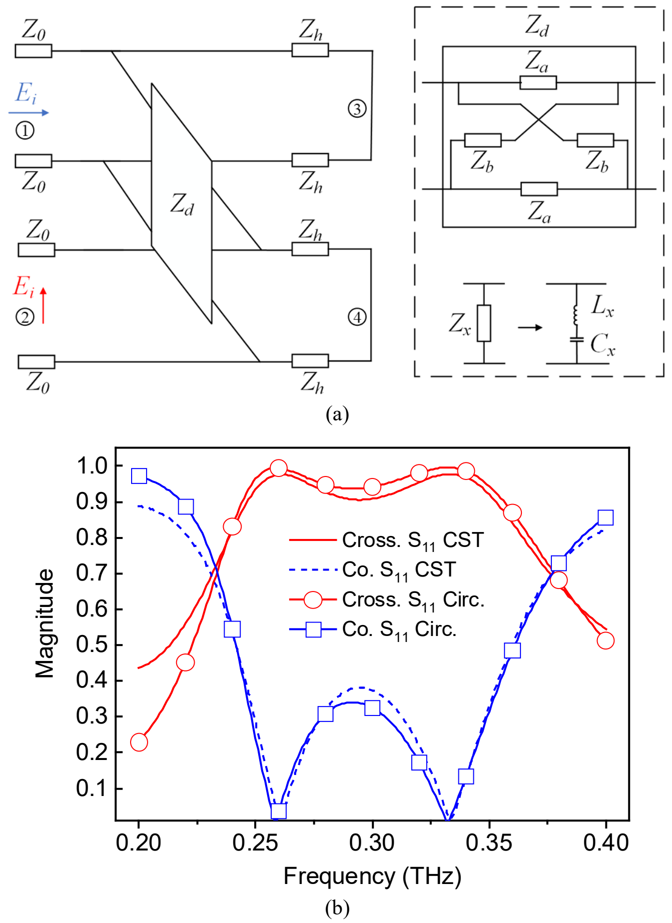

Fig. 3. (a) Equivalent circuit of the proposed cross-polarization converter. (b) Reflection coefficients of the polarization converter obtained by full-wave simulation and equivalent circuit analysis.

The proposed unit cell shown in Fig. 2(a) is defined as the "Original Cell", and the "Rotated Cell" is obtained by rotating the square ring by 90° in the counterclockwise direction around the center. The top view of one pair of the unit cells and their current distribution within the polarization conversion frequency range is shown in Fig. 2(b). It is seen that their current directions along the *y*-axis are identical while opposite along the *x*-axis, which means they are opposite in phase with an inherent 180° phase difference [47]. Therefore, if the proposed unit cells with various lengths of *l* have phase responses of 0°, 45°, 90°, and 135°, the desired 3-bits phase response (0°, 45°, 90°,135°, 180°, 225°, 270°, and 315°) can be easily obtained by rotating the direction of the notched square ring.

To further analyze the operating mechanism of the proposed polarization converter, an equivalent circuit is developed, as shown in Fig. 3(a). According to the analysis in [48], equivalent circuit of any arbitrary polarization converter under normal incidence can be represented as a Bi-mode Foster's circuit. There are two orthogonal polarization directions represented by two pairs of transmission lines. Our proposed structure is backed with the ground with total reflection characteristics, therefore the ports 3 and 4 are shorted. The interconnected two-ports network for the polarization conversion functionality can be represented by a Π equivalent circuit. Our structure is

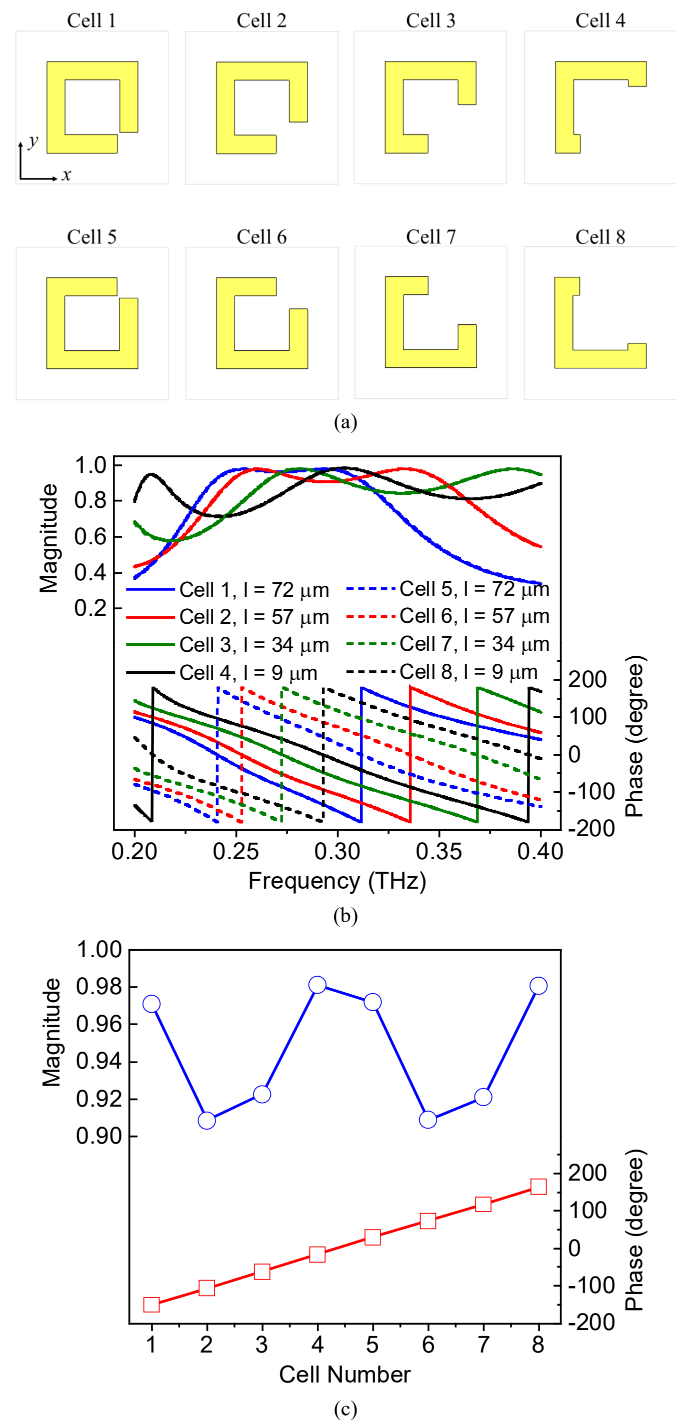

Fig. 4. Gradient phase manipulation. (a) Eight-unit cells for 360° phase shifting range. Cross-polarized reflection magnitude and phase of the unit cells (b) with different value of *l*; (c) at 300 GHz under the normal incidence.

symmetrical across the diagonal axis. Therefore, the lattice topology can be introduced, and a simple series *LC* resonator is used to model the reactance. The unit cell with the *l* value of 57 μm is taken as an example, the circuit analyzed frequency response is optimized by fitting to the full-wave simulations and the components values are extracted as: L_a = 4.3 pH, C_a = 2 fF, L_b = 5.7 pH, C_b = 0.4 fF, Z_0 and Z_h represents the characteristics impedances of the vacuum and the silicon substrate, respectively. Fig 3(b) shows the frequency responses of the

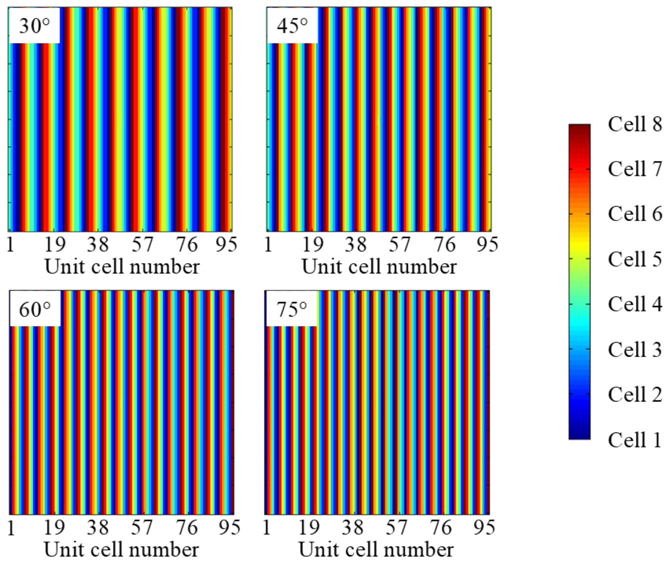

Fig. 5. Calculated reflection phase distribution of the beam-steering metasurfaces.

proposed polarization converter obtained by the full-wave simulation and the equivalent circuit analysis. The full-wave simulation is performed in CST Studio Suite, where unit cell boundary conditions were applied in the transverse directions to model the infinite periodic array, while open (add space) boundaries were assigned along the propagation direction to emulate free-space radiation, and the excitation is set as a normally incident plane wave. It is seen that the cross-polarized reflections (Cross. S_{11}) are high from 239 GHz to 365 GHz with magnitudes larger than 0.8, corresponding to low co-polarized reflections. In addition, the scattering parameters are in good agreement, which further verify the effectiveness of the equivalent circuit.

B. Phase Manipulation

To achieve the 3-bit phase responses, four variations of "Original Cell" with phase difference of 45° are needed. As mentioned before, other four desired phase status can be easily achieved by rotating the direction of the designed "Original Cell" by 90°, because there are inherent 180° phase difference between a pair of unit cells. Fig. 4(a) shows all eight variations of the notched square ring unit cells. The resonant frequency changes with the length of the current path, therefore, the value of *l* is adjusted to shift the phase response. Cells 5 to 8 are the "Rotated Cell" mode. For each pair of unit cells, their reflection magnitudes are identical, while the phase responses are opposite with a 180º phase difference.

The cross-polarized reflection magnitudes and the phase responses of the 8-unit cells are shown in Fig. 4(b). It is seen that all magnitudes maintain high around 300 GHz, and the value larger than 0.8 can be observed from 266 GHz to 323 GHz. The phase response changes with the length of *l* and the direction of the square ring with similar slopes, which ensures the robustness of the metasurface composed of these unit cells. In this work, our desired center operating frequency is 300 GHz, the performance of the unit cells at 300 GHz is shown in Fig. 4(c). It is seen that the reflection magnitudes remain higher than 0.9, while the reflection phase responses change with a total variation of 315° (the 360° phase variation is identical with 0°). As a result, the desired 3-bit reflective metasurface operating at 300 GHz can be designed by using the proposed 8-unit cells.

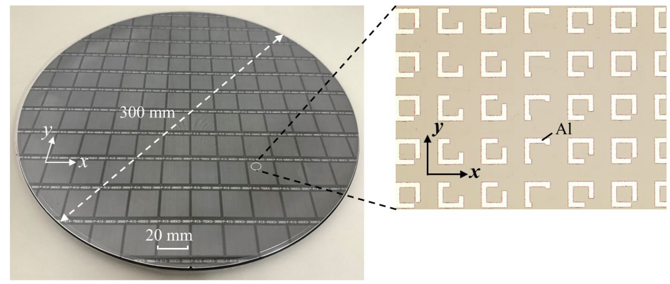

(a)

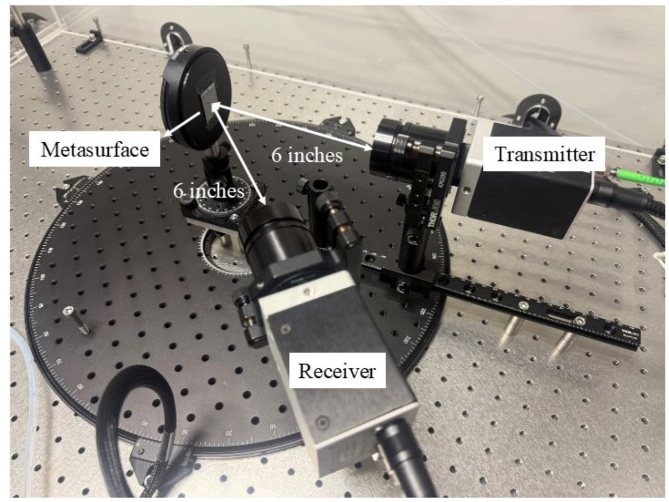

(b)

Fig. 6. Prototype and measurement setups. (a) Prototype and the microscope image of the fabricated metasurfaces. (b) Measurement setups based on THz time-domain spectroscopy.

III. Metasurface Design Procedures

To steer the direction of the reflected beam, the phase distribution ϕ_{nm}, where n and m represent the pixels in the array along the metasurface, should satisfy the following equation:

$$\phi_{nm} = \phi_r(x_n, y_m) - \phi_i(x_n, y_m) \tag{1}$$

where $\phi_r(x_n, y_m)$ and $\phi_i(x_n, y_m)$ are the phase response at the (x_n, y_m) position along the surface established by the desired reflected wave and the incident wave, respectively. The incident wave is assumed to be a normal incident plane wave, therefore, $\phi_i(x_n, y_m)$ are identical for each element, and hence can be ignored. According to the ray tracing theory [49], the phase distribution along the metasurface can be calculated by the following equation:

$$\phi_{nm} = -k\sin(\theta_r)[x_n\cos(\varphi_r) + y_m\sin(\varphi_r)] \tag{2}$$

where k is the propagation constant, and (φ_r, θ_r) is the reflected beam direction along azimuthal and elevation directions. Eight element states of "Cell 1" to "Cell 8" are defined for the 3-bit reflective beam steering according to the calculated phase

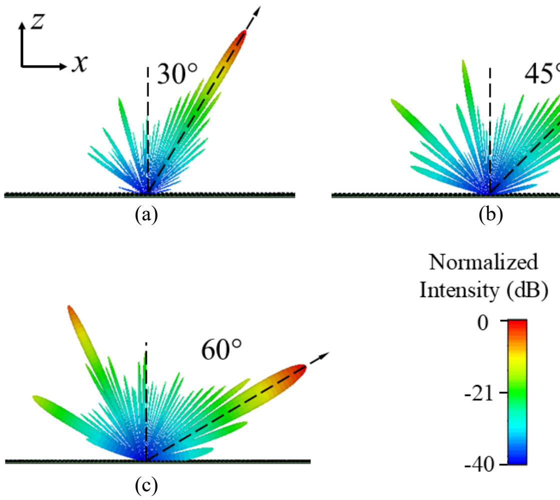

Fig. 7. Simulated cross-polarized 3-D far-field scattering patterns of (a) MS30, (b) MS45, (c) MS60 at 300 GHz. (MS=Metasurface)

distribution, for example, the element is set to "Cell 1" when the phase required is $0° \leq \phi_{nm} < 45°$, and set to "Cell 2" when $45° \leq \phi_{nm} < 90°$ and so. The required reflection phase distribution of 1.995×1.995 cm metasurfaces composed of 95×95-unit cells for the beam steering angle of $\theta_r = 30°$, 45°, 60°, and 75° ($\varphi_r = 0°$) are shown in Fig. 5 as demonstrations.

IV. Experimental Results and Discussions

A. Prototypes and Measurement Setups

Four metasurfaces (MSs) with different steering angles were fabricated and named as MS30, MS45, MS60, and MS75, respectively, to experimentally validate the beam steering performance. Fig. 6(a) shows the whole wafer with a diameter of 300 mm and the zoomed-in view of the fabricated Al notched square ring patterns under the microscope.

The THz reflective beam steering measurement was conducted using the THz time-domain spectroscopy, as shown in Fig. 6(b). A pair of linearly polarized THz antennas integrated lenses are used to transmit and receive signals, and the transmitted wave is a collimated quasi-plane wave that illuminates an area of about 1 cm in diameter. The distance between the antennas and the metasurface is around 6 inches, which is larger than 150 λ at the operating frequency of 300 GHz, and the incident wave is regarded as an *x*-polarized plane wave. A *y*-polarized receiver antenna, identical to the transmitter antenna but rotated by 90° in orientation, is placed on a turntable to measure the cross-polarized reflection. For the angle-resolved measurements, the rotating angle range is from -90° to +90° with a step of 5° for most cases, while smaller steps of 2° were used closer to the desired beam angles. It should be mentioned that for normal incidence, the feed blockage will occur in the angular region of ±27°. The measured cross-polarized reflection from the metasurfaces is normalized with the normal incident co-polarized transmitted intensity. This reference signal is obtained by aligning the pair of antennas face-to-face at 12 inches (matching the total path length in the measurement setup) without the sample holder, representing the maximum achievable system intensity at this distance. The frequency-domain signal is obtained by converting the time-domain signal through the Fourier transform.

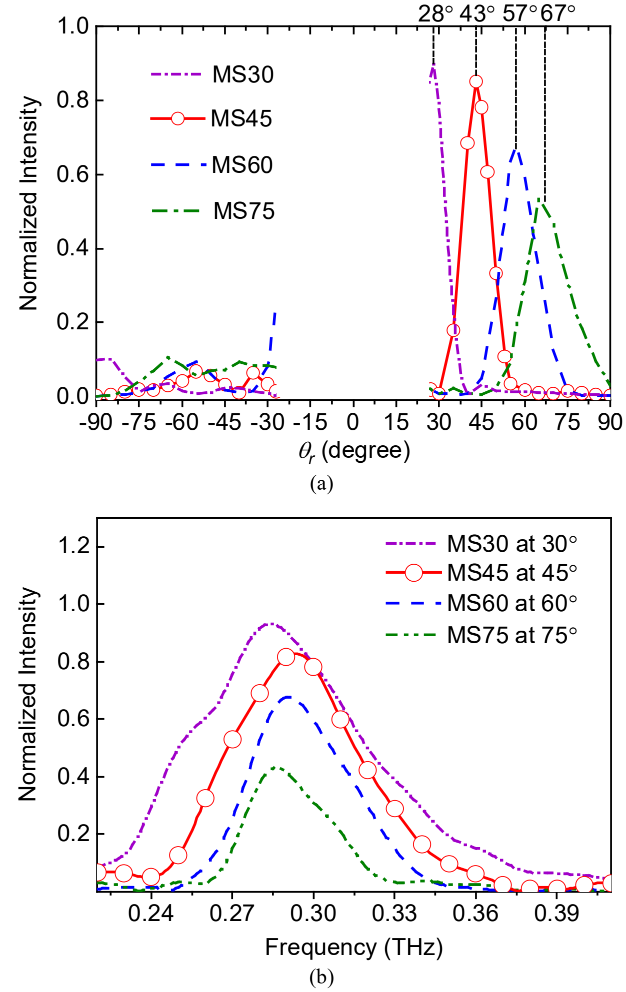

Fig. 8. Beam-scanning for cross-polarized reflection. (a) Normalized far-field scatting patterns presenting beam-scanning performance from 30° to 75° in the step of 15° at 300 GHz. (b) Normalized reflection intensities in frequency domain. (MS=Metasurface)

B. Beam Steering Performance

The simulated normalized cross-polarized 3-D far-field scattering patterns at 300 GHz in CST software with open (add space) boundaries are shown in Fig. 7. It is seen that the main lobes appear at the desired angles. For the MS30 and MS45, the side-lobe levels are below -13 dB. As for the case of beam steering to large angles up to 60°, the side-lobe level is deteriorated, which is around -5 dB. This degradation is mainly attributed to the periodic supercell coding (the coding sequence is periodically repeated), which introduces grating lobes (grating spatial harmonics) [50].

The measured beam steering performances of four metasurfaces at the desired operating frequency of 300 GHz are shown in Fig. 8(a). It is seen that the reflection beams are steered close to the desired angles. The slight angle deviations can be due to fabrication variations and experimental errors, such as a slight misalignment of the incident beam from the ideal normal incidence. For MS60, an increased intensity can be observed around -30°, which agrees with the simulated position of the large side lobe, while the maximum reflection intensity still achieves 0.68. It can also be noted that the steered beam intensity decreases with increasing steering angles, as expected.

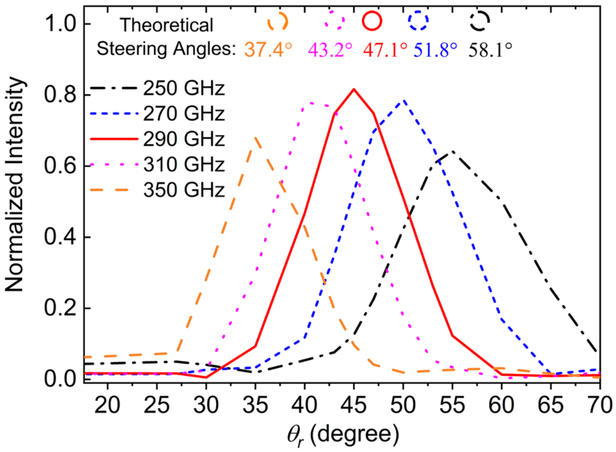

(a)

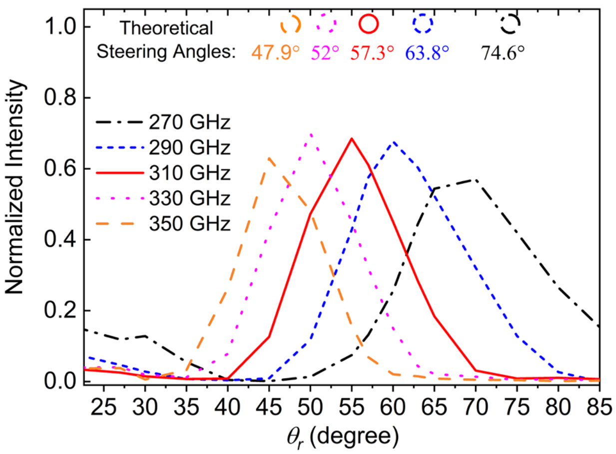

(b)

Fig. 9. Normalized radiation patterns of the (a) MS45 and (b) MS60 at various frequencies showing continuous frequency-scanning capability.

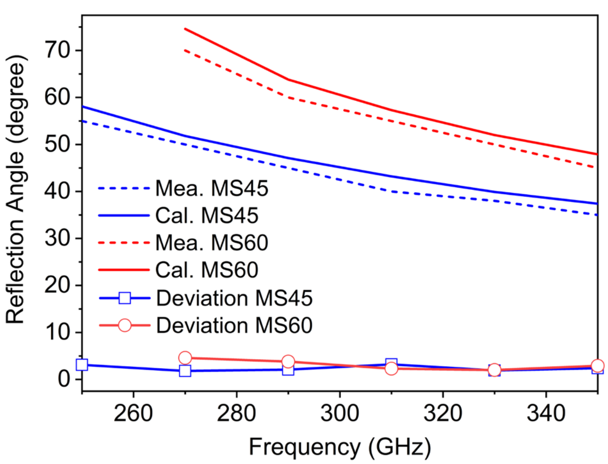

Fig. 10. Comparison between the calculated reflection angles and the measured angles for MS45 and MS60.

Fig. 8(b) shows the measured reflection intensities of the metasurfaces at the specific angles in the frequency domain. Theoretically, the maximum reflection intensities should appear at 300 GHz, while there are slight red-shifting of peak frequency. For all metasurfaces with the predicted steering angle less than 60°, the normalized reflection intensity is larger than 0.5 within the frequency range of 279 GHz to 307 GHz, which confirms the high-efficiency characteristics of the proposed design.

C. Frequency-Scanning Capability

The metasurface consisting of unit cells with similar gradient of phase with respect to frequency can be adopted for frequency-scanning functionality. This technique enables continuous beam steering within operating frequency range under normal plane-wave incidence. The beam steering angle with respect to frequency can be estimated with the following equation [51]:

$$\theta_r = \arcsin\left(\sin\theta_i + \frac{c}{2\pi f}\frac{d\phi}{dx}\right) \qquad (3)$$

where θ_i is the incident angle, $\frac{d\phi}{dx}$ is the phase gradient along the metasurface, c is the speed of light, and f is the operating frequency. According to equation (3), One of the main challenges in achieving frequency-scanning is that the phase response of each unit cell must vary linearly with frequency. Moreover, the slope of these variations should be nearly identical across all unit cells. [25], [51]. In other words, if we ignore the effect of magnitudes, the reflected beam can scan continuously in the frequency domain when the phase gradient is independent of frequency. The phase response of our proposed unit cells based on polarization conversion have similar slope with the variation of frequency as shown in Fig. 4(b). Therefore, the proposed metasurfaces have potential application of continuous frequency-scanning. The measured scattering patterns of MS45 and MS60 are normalized and shown in Fig. 9(a) and (b), respectively. It is seen that the metasurfaces can operate from 270 GHz to 350 GHz with the scanning angle range of around 20°. The measured steering angles are close to the theoretical predictions, which verifies the frequency-scanning capability of the proposed metasurfaces.

To further quantitative evaluate the scanning linearity, the calculated reflection angles according to equation (3) and measured reflection angles, together with their deviations, are compared in Fig. 10 for the MS45 and MS60 cases. The results show that the deviations remain within 5° across the entire operational frequency band, indicating good agreement with the theoretical prediction. Therefore, the proposed metasurfaces exhibit a linear and predictable frequency-scanning behavior.

D. Experimental Verification by the Metasurface Integrated Non-line-of-sight THz Communication Link

To assess the practical capabilities of the proposed metasurface, we experimentally measured the impact of beam steering metasurfaces in a non-line-of-sight THz communication link. The THz communication setup with MS75 is shown in Fig. 11, where the same testbed type [46] is used. A photomixing approach is employed to generate modulated THz signals. The transmitter consists of two continuous-wave lasers: Laser 1 serves as a local oscillator; Laser 2 is modulated using an I/Q Mach-Zehnder modulator driven by an arbitrary waveform generator (AWG) to produce two 12.5 Gbaud baseband data (I and Q) with advanced modulation formats such as quadrature amplitude modulation with 16 states (QAM-16). The 2 optical signals are then coupled

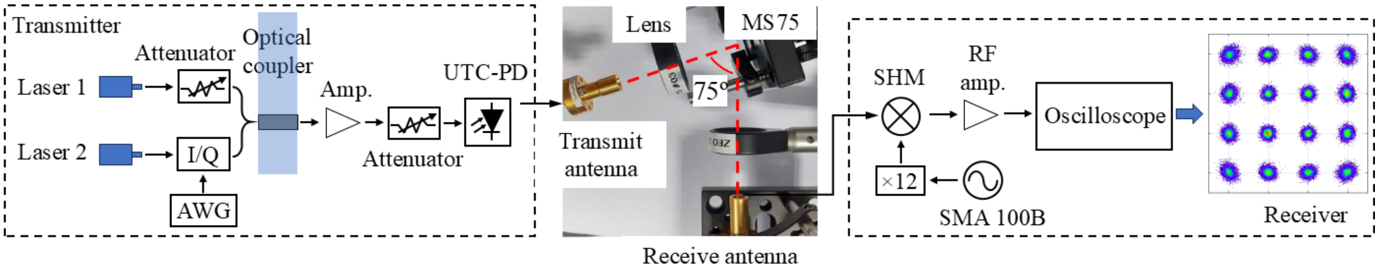

Fig. 11. Measurement setups of the proposed metasurfaces within a non-link-of-sight THz link.

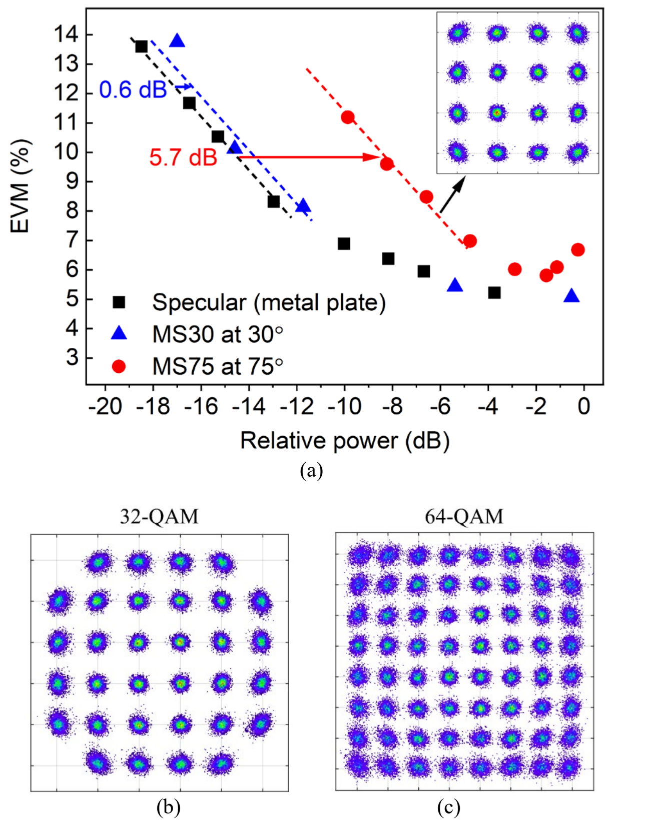

Fig. 12. (a) Error vector magnitudes (EVMs) of single-link cases for 16-QAM modulations; Constellation diagrams for (b) 32-QAM and (c) 64-QAM modulation of MS60. (MS=Metasurface)

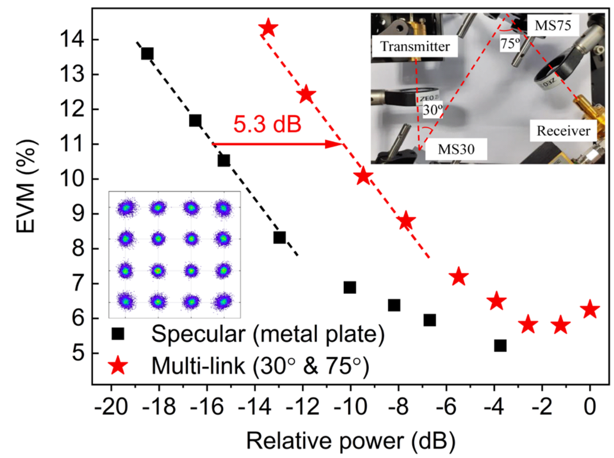

Fig. 13. Error vector magnitudes (EVMs) for 16-QAM modulations of multi-MS-link case. (MS=Metasurface)

and amplified before being fed into a uni-traveling-carrier photodiode (UTC-PD) to generate a THz signal around 300 GHz. This THz wave is radiated into the free-space using a transmit antenna (24.5 dBi gain at 300 GHz), collimated using a THz lens and reflected by MS75 to create a non-specular beam, collected by a second THz lens and sent to the receiving antenna (same type that transmit antenna), creating a THz non-line-of-sight path. At the receiver side, a subharmonic mixer (SHM) is used to downconvert the incoming THz signal to an intermediate frequency (IF) below 40 GHz. The mixer is driven by a local oscillator around 150 GHz, provided by a signal generator (SMA100B) and multiplied by a factor of 12. The downconverted signal is amplified and recorded by a high-speed oscilloscope for real-time analysis. The error vector magnitude (EVM) is evaluated using digital signal processing.

To evaluate the metasurface performance, the power penalties under the expected angular configurations are assessed, as illustrated in Fig. 12. The back-to-back setup correspond to the use of a purely specular reflector (THz mirror), where the THz path is a line-of-sight link with the 2 lenses and the mirror. The back-to-back case serves as the reference for the relative power. Thus, EVM results under specular reflection from a same-size metal plate and non-specular reflection from the metasurfaces are compared to determine the power penalty, defined as the additional power required to achieve the same EVM from line-of-sight (mirror) to non-line-of-sight with the metasurface.

Fig. 12(a) shows the QAM-16 performance for the specular reflection scenario and the non-specular reflections from individual beam-steering metasurfaces. It is seen that for MS75, the power penalty is 5.7 dB, which is still acceptable. It should be mentioned that the 75º configuration is the worst case because of the lowest intensity and the largest steering angle deviation. Modulation can be well achieved with tolerable power penalty using MS75, which indicates that the proposed metasurfaces with steering angles below 75° can easily support 16-QAM-based THz links. For example, the power penalty for MS30 is only around 0.6 dB, which is very close to the specular reflection from the metal plate. Therefore, the high efficiency of the beam steering performance achieved based on the proposed design concept is further verified in the THz link system.

Furthermore, the higher-order modulations are also evaluated using MS60, and the constellation diagrams for the 32-QAM and 64-QAM modulations corresponding to the data rates of 62.5 and 75 Gbps are shown in Fig. 12(b) and (c), respectively. Quantitatively, the measured EVM is 4.1% for the 32-QAM and 4.2% for the 64-QAM. Besides, the

TABLE I
COMPARISON OF THE PROPOSED THZ METASURFACE BASED ON CROSS-POLARIZATION CONVERSION CONCEPT WITH REPORTED THZ REFLECTIVE BEAM STEERING METASURFACES IN THE LITERATURE

Ref.	Freq. (GHz)	Fractional B.W.	Res.	Thick.	Max. beam steering angle	Freq. scanning
[15]	330	15%	Cont.	1.5 λ	45°	/
[19]	330	/	Cont.	0.5 λ	45°	/
[21]	400	Single freq. point	2-bit	0.1 λ	68°	/
[22]*	425	Single freq. point	1-bit	0.23 λ	42.8°	/
[23]*	340	Single freq. point	1-bit	0.23 λ	60°	/
[26]	1000	**31.6%**	Cont.	0.1 λ	15.2°	Yes
This work	**300**	**25.8%**	**3-bit**	**0.06 λ**	**60°**	**Yes**

* Active metausrface designs; Freq. = Frequency, B.W. = bandwidth, Res. = Resolution, Thick. = Thickness, Cont. = Continuous.

corresponding bit error rates (BERs) are 3.8×10^{-5} and 1.2×10^{-3}, respectively. Both are below typical thresholds for soft-decision forward-error correction (SD-FEC) of 2×10^{-2}, and hard-decision forward-error correction (HD-FEC) of 2×10^{-3}. The high-quality constellations indicate that the proposed metasurfaces have robust performance even under such high-order modulations. Therefore, they can readily support lower-order modulations, such as QPSK or 16-QAM, which are more commonly used in practical THz scenarios.

In addition, a multi-metasurface link based non-line-of-sight was experimentally verified by incorporating MS30 and MS75 in the same link, which can further verify the metasurfaces' ability to enhance signal spatial coverage. The QAM-16 performance for the multi-metasurface link non-specular reflection and the specular case is compared in Fig. 13. It can be observed that the constellation diagram is clear, and the power penalty of the THz link composed of MS30 and MS75 is about 5.3 dB. This further verifies that our proposed metasurfaces can work stably in various non-line-of-sight links and the effectiveness at such a wide angle steering range of 75º.

E. Comparison

To further highlight the benefits of the proposed metasurface, Table I provides a comparison with previously reported reflective THz beam steering metasurface designs. Compared with most existing metasurfaces with beam steering capability operating at only one frequency point, the proposed metasurface is more robust because the composed unit cells have stable performance in a wide frequency range. The resolution of the proposed design is relatively high with 8-unit cells (3-bit), which is beneficial to decrease the phase errors, thereby concentrating more power into the intended direction and improving the steering accuracy. Furthermore, the thickness of the metasurfaces is smaller compared with others. Although it is verified that the proposed metasurface with a 75º steering angle can well support the non-line-of-sight THz link system, the maximum beam steering angle in this work is determined to be 60º because a large sidelobe appears. To further suppress the sidelobe and increase the steering angle, it is possible to consider optimizing the coding sequence to minimize the undesired harmonics and optimizing the unit cell geometry to reduce the mutual coupling. Furthermore, the continuous frequency-scanning capability achieved with the proposed metasurface is attributed to the unit cells' similar slope of the phase response with respect to frequency.

In summary, the proposed THz metasurface achieves relatively wide-angle beam steering with high reflection efficiency. Compared with other designs, the thickness of the proposed metasurface is smaller, and the robustness is improved. The proposed design concept can be potentially applied to THz beam steering in 6G communication systems. Beyond the passive beam steering functionality, the proposed design concept can be further extended toward reconfigurable metasurfaces by integrating active switches such as vanadium dioxide (VO_2), microelectromechanical systems (MEMS), and graphene.

V. CONCLUSION

A terahertz beam-steering metasurface based on polarization conversion has been demonstrated from the aspects of beam-scanning, frequency-scanning, and the effectiveness in an actual non-line-of-sight THz link. The proposed 3-bit phase controllable unit cells achieve 360° full phase coverage and maintain high cross-polarized reflection magnitudes higher than 0.8 from 266 GHz to 323 GHz. Equivalent circuit model was also developed to validate the proposed design. Four metasurfaces composed of proposed unit cells with steering angles of 30º, 45º, 60º, and 75º at 300 GHz are experimentally demonstrated. The maximum normalized reflection intensity of the metasurface with the steering angle of 60° can still maintain 0.68, thus confirming the high efficiency characteristic. Owing to the quasi-linear phase responses of the unit cells, the metasurfaces were adopted for continuous frequency scanning from 270 GHz to 350 GHz. The metasurfaces are further verified in a non-line-of-sight THz link system. As a result, 16-QAM, 32-QAM, and 64-QAM modulations were realized by single metasurface enabled THz links. A multi-metasurface based link was also experimentally demonstrated by combining 30º and 75º metasurfaces (MS30 and MS75), and the power penalty is 5.3 dB when a 16-QAM modulation is evaluated. The proposed metasurfaces have potential applications of THz beam steering components in future 6G communication systems as well as the THz imaging systems.

REFERENCES

[1] J. Zhang, G. Wu, M. Chen, X. Liu, K. Chan, D. Tsai and C. Chan, "A 6G meta-device for 3D varifocal," *Sci. Adv.,* vol. 9, Jan. 2023, Art. no. eadf8478.

[2] H. Yang, S. Zheng, H. Zhang, N. Li, D. Shen, T. He, Z. Yang, Z. Lyu and X. Yu, "A THz-OAM wireless communication system based on transmissive metasurface," *IEEE Trans. Antennas Propag*., vol. 71, no. 5, pp. 4194-4203, May 2023.

[3] W. Jiang, Q. Zhou, J. He, M. A. Habibi, S. Melnyk, M. El-Absi, B. Han, M. D. Renzo, H. D. Schotten, F.-L. Luo, T. S. El-Bawab, M. Juntti, M. Debbah and V. C. M. Leung, "Terahertz communications and sensing for

6G and beyond: a comprehensive review," *IEEE Commun. Surveys Tuts.*, vol. 26, no. 4, pp. 2326-2381, Apr. 2024.

[4] D. Serghiou, M. Khalily, T. W. C. Brown and R. Tafazolli, "Terahertz channel propagation phenomena, measurement techniques and modeling for 6G wireless communication applications: a survey, open challenges and future research directions," *IEEE Commun. Surveys Tuts.*, vol. 24, no. 4, pp. 1957-1996, Sep. 2022.

[5] J. M. Jornet, E. W. Knightly and D. M. Mittleman, "Wireless communications sensing and security above 100 GHz," *Nature Communications*, vol. 14, no. 1, Feb. 2023.

[6] Y. Liu, Y. Wang, X. Fu, L. Shi, F. Yang, J. Luo, Q. Zhou, Y. Fu, Q. Chen, J. Dai, L. Zhang, Q. Cheng and T. Cui, "Toward sub-terahertz: Space-time coding metasurface transmitter for wideband wireless communications," *Adv. Sci.*, vol. 10, no. 29, Oct. 2023, Art. no. 2304278.

[7] C. Lin and G. Y. Li, "Indoor terahertz communications: How many antenna arrays are needed?," *IEEE Trans. Wireless Commun.*, vol. 14, no. 6, pp. 3097-3107, June 2015.

[8] L. Dai, J. Tan, Z. Chen and H. V. Poor, "Delay-phase precoding for wideband THz massive MIMO," *IEEE Trans. Wireless Commun.*, vol. 21, no. 9, pp. 7271-7286, Sep. 2022.

[9] D. W. Prather, J. A. Murakowski, C. Schuetz, S. Shi, G. J. Schneider and C. Harrity, "Millimeter-wave and sub-THz phased-array imaging systems based on electro-optic up-conversion and optical beamforming," *IEEE J. Sel. Topics Quantum Electron*., vol. 29, no. 5, Sep. 2023, Art. no. 8501014.

[10] M. Che, K. Kondo, H. Kanaya, and K. Kato, "Arrayed photomixers for THz beam-combining and beam-steering," *J. Lightw. Technol.,* vol. 40, no. 20, pp. 6657–6665, Oct. 2022.

[11] T. Haddad, C. B. Quel, P. Lu, J. Tebart, B. Sievert, S. Makhlouf, M. Grzeslo, J. Teniente, C. D. Río, and A. Stöhr, "Photonic-assisted 2-D terahertz beam steering enabled by a LWA array monolithically integrated with a BFN," *Opt. Express*, vol. 30, no. 21, pp. 38596-38612, Oct. 2022.

[12] M. Deng, M. Cotrufo, J. Wang, J. Dong, Z. Ruan, A. Alù, and L. Chen, "Broadband angular spectrum differentiation using dielectric metasurfaces," *Nature Commun.*, vol. 15, no. 1, Mar. 2024, Art. no. 2237.

[13] C. Rong, L. Wu, J. Tao, Y. Cheng, K. Wang, and L. Chen, "Metasurface-based optical neural network and its application in next-generation optical communications and networks," *J. Lightw. Technol.*, vol. 43, no. 18, pp. 8538-8562, Sep. 2025.

[14] X. Fu, F. Yang, C. Liu, X. Wu and T. J. Cui, "Terahertz beam steering technologies: From phased arrays to field-programmable metasurfaces," *Adv. Opt. Mater.*, vol. 8, no. 3, Feb. 2020, Art. no. 1900628.

[15] A. Ali, M. Khalily, T. Brown, and R. Tafazolli, "Metasurface-based THz reflectarray antenna with vortex multiplexing and beam-steering capabilities for future wireless communications," *iScience*, vol. 25, no. 8, Aug. 2022, Art. no. 104725.

[16] F. Taleb, G. G. Hernandez-Cardoso, E. Castro-Camus and M. Koch, "Transmission, reflection, and scattering characterization of building materials for indoor THz communications," *IEEE Trans. Terahertz Sci. Technol.*, vol. 13, no. 5, pp. 421-430, Sep. 2023.

[17] A. A. Baba, R. M. Hashmi, K. P. Esselle, M. Attygalle and D. Borg, "A millimeter-wave antenna system for wideband 2-D beam steering," *IEEE Trans. Antennas Propag*., vol. 68, no. 5, pp. 3453-3464, May 2020.

[18] S. Huang, K. Y. Chan and R. Ramer, "All 3-D printed antennas based on phase velocity control for beam steering and size reduction with low cost," *IEEE Trans. Antennas Propag*., vol. 70, no. 3, pp. 1776-1786, Mar. 2022.

[19] A. Ali, M. Khalily, T. Brown, and R. Tafazolli, "Metasurface-based THz reflectarray antenna with vortex multiplexing and beam-steering capabilities for future wireless communications," *iScience*, vol. 25, no. 8, Aug. 2022, Art. no. 104725.

[20] A. Monti, A. Alù, A. Toscano and F. Bilotti, "Surface impedance modeling of all-dielectric metasurfaces," *IEEE Trans. Antennas Propag*., vol. 68, no. 3, pp. 1799-1811, Mar. 2020.

[21] L. Y. Wang, F. Lan, Y. X. Zhang, S. X. Liang, W. X. Liu, Z. Q. Yang, L. Meng, Z. J. Shi, J. Yin, T. T. Song, H. X. Zeng, and P. Mazumder, "A fractional phase-coding strategy for terahertz beam patterning on digital metasurfaces," *Opt. Express*, vol. 28, no. 5, pp. 6395–6407, Mar. 2020.

[22] B. Chen, X. Wang, W. Li, C. Li, Z. Wang, H. Guo, J. Wu, K. Fan, C. Zhang, Y. He, B. Jin, J. Chen and P. Wu "Electrically addressable integrated intelligent terahertz metasurface," *Sci. Adv.*, vol. 8, no. 41, Oct. 2022, Art. no. eadd1296.

[23] F. Lan, L. Wang, H. Zeng, S. Liang, T. Song, W. Liu, P. Mazumder, Z. Yang, Y. Zhang and D. M. Mittleman "Real-time programmable metasurface for terahertz multifunctional wave front engineering," *Light: Sci. Appl*., vol. 12, no. 1, p. 191, Aug. 2023.

[24] S. Kuznetsov, M. Tumashov, V. K. Killamsetty, P. Lazorskiy, A. Epstein and S. Glybovski, "Efficient anomalous refraction of THz beams with a multilayer metal–polymer huygens' metasurface," *IEEE Trans. Terahertz Sci. Technol.*, vol. 14, no. 1, pp. 109-121, Jan. 2024.

[25] L. Song, T. Zhang, P.-Y. Qin, J. Du and Y. J. Guo, "Sub-THz broadband transmitting metasurfaces with enhanced frequency-scanning capability," *IEEE Trans. Terahertz Sci. Technol.*, vol. 14, no. 1, pp. 82–90, Jan. 2024.

[26] C. Yang, G.-B. Wu, B. Chen, K. F. Chan, and C. H. Chan, "Terahertz Bessel beam scanning enabled by dispersion-engineered metasurface," *IEEE Trans. Microw. Theory Techn.*, vol. 71, no. 8, pp. 1–9, Aug. 2023.

[27] X. You, R. T. Ako, S. Sriram, and W. Withayachumnankul, "3D terahertz confocal imaging with chromatic metasurface," *Laser Photon. Rev.*, vol. 19, no. 7, pp. 1–2401011, Apr. 2025.

[28] Z. Huang, Z. Wang, Y. Cheng, X. Li, J. Wang, L. Zhou, H. Xu, X. Luo, and L. Chen, "Metasurfaces empower optical multiparameter imaging: A review," *Sci. China Phys., Mechan. Astron.*, vol. 68, no. 7, 2025, Art. no. 274201.

[29] H. Huang and Z. Shen, "Low-RCS reflectarray with phase controllable absorptive frequency-selective reflector," *IEEE Trans. Antennas Propag*., vol. 67, no. 1, pp. 190-198, Jan. 2019.

[30] X. Zhang, F. Yang, S. Xu, A. Aziz and M. Li, "Dual-layer transmitarray antenna with high transmission efficiency," *IEEE Trans. Antennas Propag*., vol. 68, no. 8, pp. 6003-6012, Aug. 2020.

[31] G. Isic, D. C. Zografopoulos, D. B. Stojanovic, B. Vasic and M. R. Belic, "Beam steering efficiency in resonant reflective metasurfaces," *IEEE J. Sel. Topics Quantum Electron.*, vol. 27, no. 1, Jan./Feb. 2021, Art. no. 4700208.

[32] M. Li and Z. Shen, "Low-RCS transmitarray based on 2.5-D cross-polarization converter," *IEEE Trans. Antennas Propag*., vol. 71, no. 7, pp. 5828-5837, Jul. 2023.

[33] F. Qin, Y. Liu, C. Gu, L. Zeng, W. Cheng, H. Zhang and S. Gao, "Multibeam hybrid transmitarray based on polarization rotating metasurface with reconfigurable bidirectional radiation," *IEEE Trans. Antennas Propag*., vol. 72, no. 9, pp. 6992-7004, Sep. 2024.

[34] J. Hu, C. Wang, M. Deng, L. Deng, H. Wong and L. Sang, "A dual-channel linear-to-circular polarization conversion transmitarray with independent wavefront control capability," *IEEE Trans. Microw. Theory Techn.*, vol. 72, no. 12, pp. 7039–7049, Dec. 2024.

[35] M. Wang, M. T. Yim and C. H. Chan, "Dual-polarized folded reflectarray antenna with active components," *IEEE Trans. Antennas Propag*., vol. 72, no. 6, pp. 5289-5294, June 2024.

[36] W. Fu, Y. Cai, P. Mei, G. Frølund Pedersen and S. Zhang, "Electronically reconfigurable filtering reflectarray antenna using polarization conversion elements with controllable conversion zeros," *IEEE Trans. Antennas Propag*., vol. 72, no. 9, pp. 7359–7364, Sep. 2024.

[37] W. Liu, L. Deng, L. Chen, C. Zhang and S. Li, "A broadband high-gain low-profile folded transmitarray antenna for OAM generation," *IEEE Antennas Wireless Propag. Lett*., vol. 23, no. 12, pp. 4348-4352, Dec. 2024.

[38] T. Huang, Z. Wu, S. Huang, Z. Wen, W. Jiang and J. Xu, "Broadband transreflective metasurface for multifunctional dual-band OAM engineering," *IEEE Trans. Antennas Propag.*, vol. 72, no. 9, pp. 7041-7047, Sep. 2024.

[39] Y. Wang, S. Li, H. Wang, L. Feng, B. Tan, Y. Tan, R. Su, J. Wu, C. Zhang, B. Jin, J. Chen and P. Wu, "Broadband and efficient asymmetric wavefront manipulation via terahertz polarization-selective metasurface," *Appl. Phys. Lett.*, vol. 121, no. 15, Oct. 2022, Art. no. 151701.

[40] X. You, R. T. Ako, M. Bhaskaran, S. Sriram, C. Fumeaux, and W. Withayachumnankul, "Mechanically tunable terahertz circular polarizer with versatile functions," *Laser Photon. Rev.*, vol. 17, no. 4, Feb. 2023, Art. no. 2200305.

[41] M. Yang, Z. Song, F. Hu, D. Wei and Z. Yang, "Ultra-broadband terahertz polarization converter based on flexible metamaterial," *Appl. Phys. Lett.* Vol. 126, no. 12, Mar. 2025, Art. No. 121701.

[42] Z. Xing, S. Liao, Y. Zheng, X. Tang, and H. Zhang, "Terahertz dual-mechanism dual-band linear-to-circular polarization converter with one-octave band separation and orthogonal polarization," *Opt. Exp*., vol. 33, no. 7, pp. 14777-14795, Mar. 2025.

[43] G. Deng, Y. Zhu, Q. Zhang, J. Yang, Y. Li and Z. Yin, "Reconfigurable dual-functional reflective polarization converter based on liquid crystal terahertz metasurfaces," *IEEE Trans. Antennas Propag*., vol. 73, no. 6, pp. 4164-4169, Jun. 2025.

[44] L. Cong, Y. K. Srivastava, H. Zhang, X. Zhang, J. Han, and R. Singh, "All-optical active THz metasurfaces for ultrafast polarization switching and dynamic beam splitting," *Light Sci. Appl.*, vol. 7, no. 1, p. 28, 2018.

[45] F. Yang, T. C. Tan, S. Prakash, A. Kumar, A. Ariando, R. Singh, N. Wang and P. Pitchappa, "Reconfigurable wide-angle beam-steering terahertz metasurfaces based on vanadium dioxide," *Adv. Opt. Mater.*, vol. 12, no. 9, Mar. 2024, Art. no. 2302047.

[46] F. Dutin, U. B. Gartzia, V. Torres, P. Szriftgiser, J. Teniente and G. Ducournau, "Non-line-of-sight 300 GHz band wireless link enabled by a frequency dependent reflective surface," *IEEE Trans. Terahertz Sci. Technol.*, vol. 15, no. 3, pp. 400-411, May 2025.

[47] L. Zhou and Z. Shen, "Hybrid frequency-selective rasorber with low-frequency diffusion and high-frequency absorption," *IEEE Trans. Antennas Propag*., vol. 69, no. 3, pp. 1469-1476, Mar. 2021.

[48] G. Perez-Palomino and J. E. Page, "Bimode Foster's equivalent circuit of arbitrary planar periodic structures and its application to design polarization controller devices," *IEEE Trans. Antennas Propag.*, vol. 68, no. 7, pp. 5308–5321, Jul. 2020.

[49] J.-B. Gros, V. Popov, M. A. Odit, V. Lenets, and G. Lerosey, "A reconfigurable intelligent surface at mmWave based on a binary phase tunable metasurface," *IEEE Open J. Commun. Soc.*, vol. 2, pp. 1055–1064, May 2021.

[50] R. Mailloux, "Array grating lobes due to periodic phase, amplitude, and time delay quantization," *IEEE Trans. Antennas Propag.*, vol. AP-32, no. 12, pp. 1364–1368, Dec. 1984.

[51] N. Yu, P. Genevet, M. A. Kats, F. Aieta, J.-P. Tetienne, F. Capasso, and Z. Gaburro, "Light propagation with phase discontinuities: Generalized laws of reflection and refraction," *Science*, vol. 334, no. 6054, pp. 333–337, Oct. 2011.